coatings

MDPI

Article

Tailoring Al–Li Alloy Surface Wettability with a Femtosecond Laser and Its Effect on Bonding Performance

Jun Chen [1], Yibo Li [2,*], Minghui Huang [1] and Lei Dong [2]

[1] College of Mechanical and Electrical Engineering, Central South University, Changsha 410083, China; chenjun.csu@csu.edu.cn (J.C.); meeh@csu.edu.cn (M.H.)
[2] Light Alloy Research Institute, Central South University, Changsha 410012, China; 193812019@csu.edu.cn
* Correspondence: yibo.li@csu.edu.cn

Abstract: In this study, a femtosecond laser was used to pretreat the surface of the Al–Li alloy, the surface micromorphology, roughness, contact angle, and surface wettability of which were adjusted by changing the laser scanning speed, and the sample was bonded into a single joint with polyether ether ketone (PEEK) adhesive. The mechanism of the laser surface treatment affecting the bonding strength of the Al–Li alloy was explored through tensile and shear experiments. The results indicated that optimizing the laser surface treatment parameters could change the surface roughness and surface micromorphology of the Al–Li alloy, so as to change its surface free energy and bonding strength. Compared with the untreated sample, the bonding strength of the Al–Li alloy increased by 81%, 95%, 107%, 91%, and 78% under the treatment of laser scanning at 25, 20, 15, 10, and 5 mm/s, respectively. As a whole, femtosecond laser etching of the Al–Li alloy surface had an important influence on its wettability and bonding performance.

Keywords: Al–Li alloy; femtosecond laser; surface characteristics; wettability; bonding performance

Citation: Chen, J.; Li, Y.; Huang, M.; Dong, L. Tailoring Al–Li Alloy Surface Wettability with a Femtosecond Laser and Its Effect on Bonding Performance. *Coatings* **2021**, *11*, 995. https://doi.org/10.3390/coatings11080995

Academic Editors: Grzegorz Dercz and Robert B. Heimann

Received: 17 July 2021
Accepted: 16 August 2021
Published: 20 August 2021

1. Introduction

The Al alloy has excellent physical and chemical properties and is widely used in the aerospace and automotive industries. When manufacturing Al alloy parts, the connection between Al alloys is inevitable, especially when manufacturing parts with complex geometries or large dimensions [1]. At present, mechanical connection, welding, and bonding are the main methods for Al alloys connection. The mechanical connection method generally connects materials together through bolts or rivets and other fasteners, adding extra weight and causing concentrated stress within connectors. The welding operation easily produces deformation and cracks, which seriously affect properties of the material. On account of overcoming these shortcomings, the bonding technology is now being used more and more widely due to its excellent characteristics [2,3].

Surface treatment technology is usually adopted to improve the bonding strength and bonding performance of the Al alloy. Traditional surface treatment is usually carried out by mechanical sandblasting, sanding, chemical etching, and anodizing methods [4–8]. In these processes, mechanical sandblasting and polishing have limited effects. Anodizing and chemical etching are rather effective in changing the surface properties of Al alloys and improving the bonding strength, although this technology is expensive, complex, and accompanied by pollution. Compared with traditional surface treatment technology, laser surface treatment is a green and noncontact method that does not use solutions or introduce secondary pollution, which can provide a uniform surface with high reliability and repeatability [9,10], and has become a research focus in recent years.

Wan et al. [11] studied the effect of laser spot overlap rate on the surface properties and bonding strength of the AA6022–T4 Al alloy. Li et al. [12] pretreated the surfaces of the Al alloy and the carbon fiber reinforced polymer (CFRP) joint with an ultrafast picosecond infrared (IR) laser and a nanosecond ultraviolet (UV) laser and the shear strength

of the treated Al alloy/CFRP joint increased from 5.6 to 24.8 and 21.9 MPa, respectively. Spadaro et al. [13] used beams of different diameters and energy to perform laser processing on Al alloy 2024 substrates and studied the effects of irradiation conditions on the morphology of the adherend and the fracture energy of the adhesive joint. Wu et al. [14] explored the effect of laser ablation surface treatment with different energy on the performance of adhesive-bonded AA6022–T4 joints through a series of experiments. Romoli et al. [15] studied the effect of the microgrooves produced by the laser on the strength of Al alloy joints under different laser energy densities.

Although a large number of studies have begun to explore the use of laser surface treatment as a preprocess of Al alloy bonding, the research has mainly focused on picosecond and nanosecond lasers. When the pulse width is a nanosecond or longer, the subtle phase transitions and structural changes caused by photophysical and photochemical processes will be directly removed due to thermal effects such as melting and redecomposition. These shortcomings can be overcome by a femtosecond laser [16,17]; so the femtosecond laser has unique advantages and broad application prospects. However, the research on the related processes, technologies, and mechanisms of the femtosecond laser as a surface treatment technology in the bonding process is still in its infancy. In order to further study the mechanism of improving bonding strength by femtosecond laser etching, in this paper, we investigated the effect of femtosecond laser pretreatment with different laser scanning speeds on the surface morphology of the Al–Li alloy and the consequent adhesive properties between the polyether ether ketone (PEEK) adhesive and the Al–Li alloy.

2. Materials and Methods

2.1. Materials

The 2 mm thick bare Al–Li alloy (Al–Li–S–4, Alcoa, Pittsburgh, PA, USA) used in this study was sheared into pieces sized 100 mm × 25 mm; the chemical properties of the alloy are presented in Table 1. The PEEK films, with a glass transition temperature of 143 °C and a melting point of 343 °C [18], were supplied by the GEHR Company, Los Angeles, CA, USA. The mechanical properties of the PEEK and Al–Li alloy are shown in Table 2.

Table 1. Chemical compositions of the Al–Li alloy (wt.%) [19].

Fe	Si	Cu	Mn	Mg	Ag	Zn	Li	Zr	Ti	Al
0.03	0.01	3.64	0.29	0.71	0.32	0.36	0.68	0.12	0.03	Bal

Table 2. Properties of the Al–Li alloy and the PEEK.

Property	Al–Li Alloy [20]	PEEK
Tensile strength σb (MPa)	532	116 [a]
Elastic modulus (GPa)	75.9	3.73 [a]
Poisson's ratio	0.33	0.28 [18]
Elongation (%)	12.5	-

[a] tested.

2.2. Procedures

2.2.1. Sample Preparation

The femtosecond laser that was used to pretreat the surface of the Al–Li alloy had been cleaned with ethanol to modify the surface. After pretreatment, the sample was cleaned again to avoid being oxidized by air or absorbing impurity particles in the air, and then subsequent treatment (wetting measurements, bonding, and so on) was carried out.

The femtosecond laser is a titanium-doped sapphire solid state femtosecond laser amplifier system produced by Spectra Physics, Milpitas, CA, USA. The laser beam spot was circular, and the focal point was 5 μm in diameter with a wavelength of 800 nm. The laser scanning path shown in Figure 1a was selected. In this experiment, different surfaces

were obtained mainly by adjusting the scanning speed, as shown in Table 3. The other parameters of laser processing are shown in Table 4.

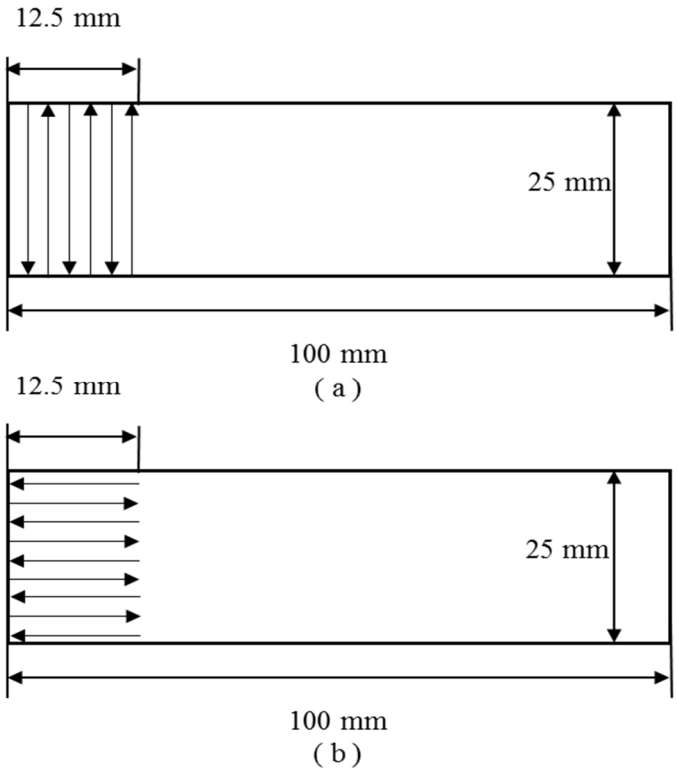

Figure 1. Laser scanning path: (**a**) perpendicular to stretching direction, (**b**) parallel to stretching direction.

Table 3. Al–Li alloy sample numbers and corresponding treatment methods.

Parameters	P-0	P-1	P-2	P-3	P-4	P-5
Scanning speed/(mm/s)	untreated	25	20	15	10	5

Table 4. Laser processing parameters.

Parameter	Value
Mean power/W	0.35 [a]
Repetition frequency/kHz	1 [b]
Pulse width/fs	120 [b]
Beam diameter/μm	5 [b]
Hatch spacing/μm	100

[a] tested; [b] manufacturer's data.

2.2.2. Bonding Test

After the femtosecond laser pretreatment, the Al–Li alloy adhesive-bonded joints were cured using a PEEK film adhesive, according to the processing process shown in Figure 2. First, a prepressure of 0.8 MPa was applied to the adhesive-bonded joint, and the purpose was to extrude the excess air in the joint structure. At the same time, heating was started until the temperature reached 390 °C, and the heat and pressure were kept for 40 min to sufficiently melt the PEEK. Then, the pressure was increased to 1.5 MPa and kept for 30 min to fully infiltrate the PEEK on the surface of the adherend. Finally, the joint was cooled down to room temperature and the pressure was released.

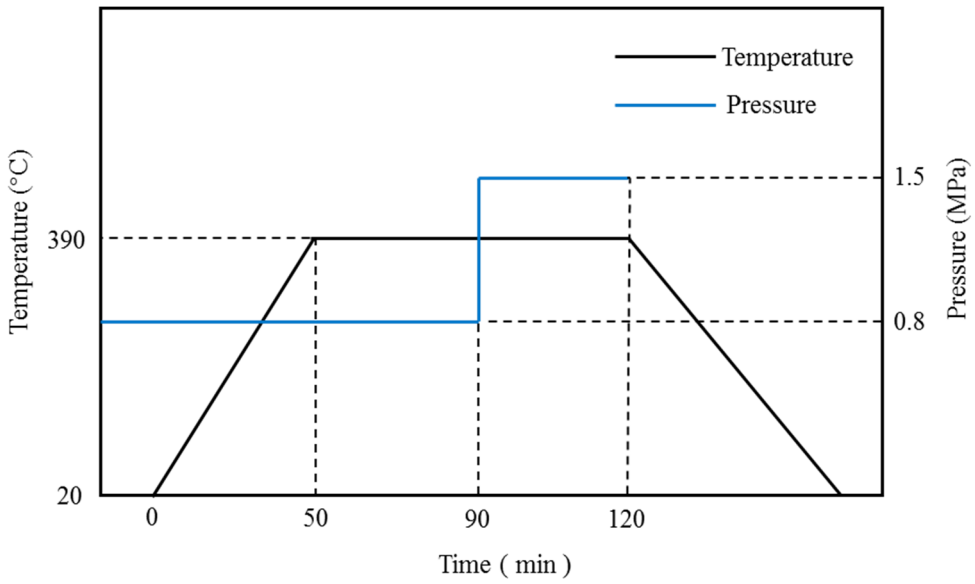

Figure 2. The schematic of the curing process for the joint.

2.3. Experimental Characterization

2.3.1. Surface Characteristics

A scanning electron microscope (SEM, TESCAN, MIRA3, Brno, Czech Republic) was used to observe the surface. To examine the surface topography, a white light profilometer (WYKO NT9100, Veeco Metrology Inc., Plainview, NY, USA) was employed.

2.3.2. Surface Wettability

Surface contact angles of different samples with liquids were detected using a Theta–Biolin contact angle meter (Biolin Scientific, Gothenburg, Sweden) to evaluate the modification of the wettability of the surface; good wettability is beneficial to the spreadability of the adhesive.

2.3.3. Shear Strength Test

Figure 3 provides the single lap shear specimen configuration, and the substrates are Al–Li alloys pretreated by the femtosecond laser. According to the testing standard of ASTM D1002-72 [21], shear strength tests were accomplished using an Instron 3369 machine. Five samples were prepared to acquire average value.

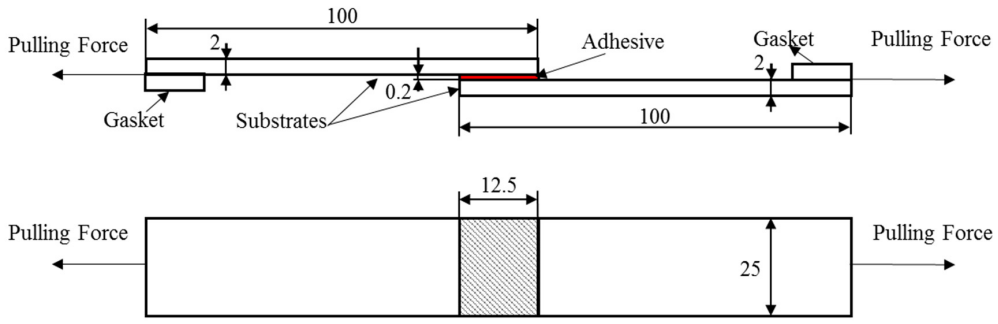

Figure 3. Form and dimensions of the single lap joint (units: mm).

3. Results and Discussion

3.1. Surface Characteristics

A white light profilometer was used to observe the surface topography after the femtosecond laser pretreatment. The R_a (surface roughness parameter) of the samples

was measured, and the valid data were recorded; then the results were averaged. As the contrast, the untreated samples were also tested. It can be seen from Figure 4 that the surface laser pretreatment significantly improved the surface roughness of the Al–Li alloy plate. The energy of the laser processing the surface of the Al alloy increased at the same position, and the surface roughness of the Al–Li alloy plate also increased as the processing speed decreased. The surface roughness of the untreated Al alloy was 0.334 μm. After laser pretreatment, the surface roughness became 0.501 μm (25 mm/s), 0.527 μm (20 mm/s), 0.821 μm (15 mm/s), 1.043 μm (10 mm/s), and 1.493 μm (5 mm/s), exhibiting an increase of 50%, 57.8%, 145.8%, 212.3%, and 347.0%, respectively. In addition, low-energy (faster scanning speed) laser pretreatment had a limited effect on the surface roughness of the Al–Li alloy, which was greatly affected by the original surface (Figure 4b,c), and no significant laser scanning traces could be seen. After high-energy (slow scanning speed) laser pretreatment (Figure 4d–f), the laser scanning traces were significant, and the surface roughness of the Al–Li alloy was mainly affected by the impact of dents left by the laser scanning.

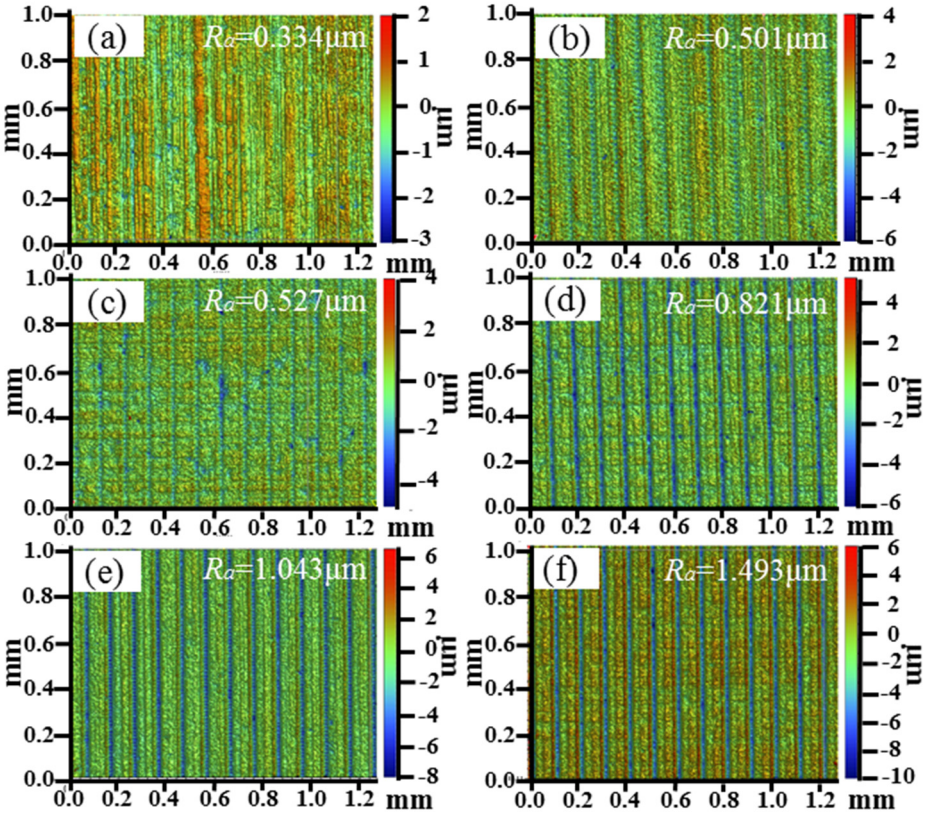

Figure 4. Surface roughness of the samples: (**a**) P-0, (**b**) P-1, (**c**) P-2, (**d**) P-3, (**e**) P-4, (**f**) P-5.

After further analyzing the surface profile of the Al–Li alloy plate sample (Figure 5), it was discovered that after the femtosecond laser scanning, the surface topography was not uniformly changed, but significant dents were formed, and the concave left by the laser scanning showed a more significant impact on the contour of the sample surface as the scanning speed decreased (greater scanning energy). The untreated Al–Li alloy surface (Figure 5a) had a relatively smooth profile, and the laser-treated Al–Li alloy surface profile was mainly affected by the groove marks and splashes left by the laser scanning. The surface profile of the Al–Li alloy fluctuated significantly, and the overall profile was relatively messy, but the dents were not significant when treated by the laser with a scanning speed of 25 mm/s (Figure 5b), 20 mm/s (Figure 5c). When the laser scanning speed was 15 (Figure 5d), 10 (Figure 5e), and 5 mm/s (Figure 5f), the outline of the Al–Li alloy after laser scanning was clear with significant regularity. At these speeds, the surface

profile of the sample was mainly affected by the groove after laser processing, and the groove depth reached 3.5, 3.9, and 4.9 μm, respectively.

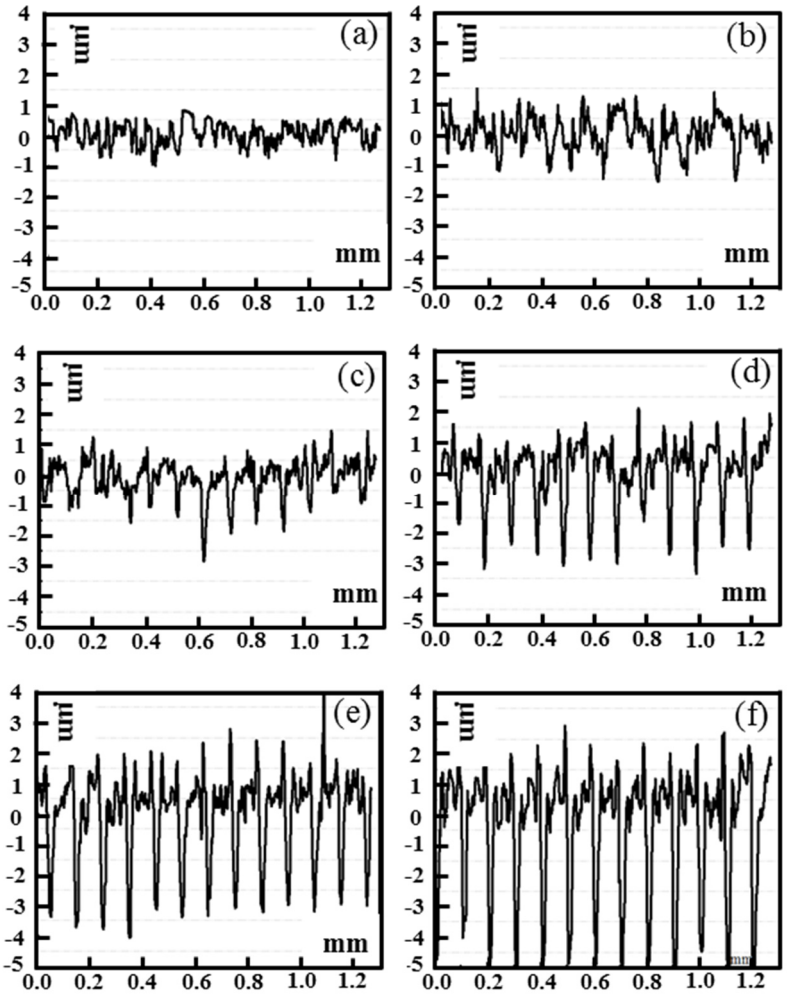

Figure 5. Surface roughness profile of the samples: (**a**) P-0, (**b**) P-1, (**c**) P-2, (**d**) P-3, (**e**) P-4, (**f**) P-5.

The surface morphology and topography of the pristine and laser-treated samples characterized by SEM are shown in Figure 6. The surface of the original Al–Li alloy (Figure 6a) was relatively flat with scratches left by rolling. The surface damage of the Al–Li alloy after laser scanning (Figure 6b–f) was significant. Compared with the untreated sample, it was observed that there were laser scanning grooves on the surface of the Al–Li alloy and splashes around the grooves. The deeper groove and more splashes were produced as the scanning speed became slower, and hence the surface roughness was greater. This is consistent with the roughness measurement results in Figure 4. A large number of nanosubstructures covering the entire microgroove surface appeared on the surface of the microscale groove due to the induction mechanism of the femtosecond laser ultrashort pulse [22,23]. It could be seen from the microscopic image inside the groove that the nanosubstructure was nanoparticles with particle sizes ranging from tens to hundreds of nanometers, which consisted mainly of the nano-oxide particles produced in the etching process. Further analysis showed that when the laser scanning speed was 25 mm/s (Figure 6b), 20 mm/s (Figure 6c), and 15 mm/s (Figure 5d), more nanoparticles were formed inside the groove significantly with the increase in the scanning speed. When the laser scanning speed was 15 mm/s (Figure 6d), 10 mm/s (Figure 6e), and 5 mm/s (Figure 6f), the nanosubstructure of the groove after laser scanning was weakened, and the color transferred to pale white. This is mainly because the excessively high laser scanning

energy caused the Al–Li alloy around the active area to be vaporized or melted, which caused thermal damage to the surrounding tissues.

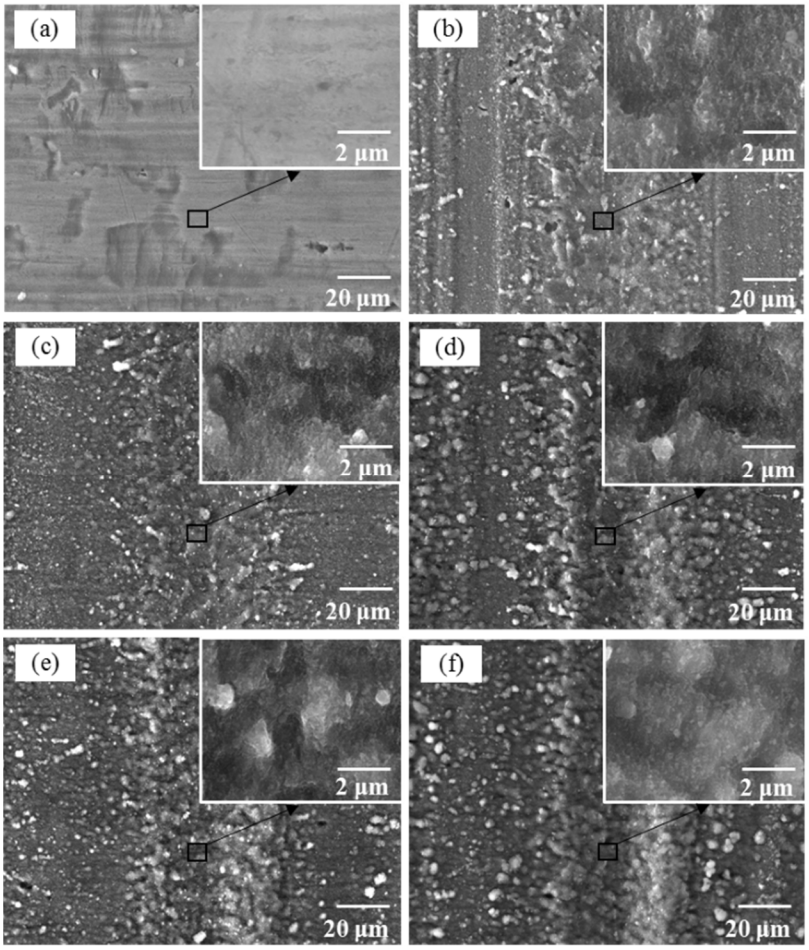

Figure 6. SEM images of the samples: (**a**) P-0, (**b**) P-1, (**c**) P-2, (**d**) P-3, (**e**) P-4, (**f**) P-5.

3.2. Contact Angle and Surface Free Energy

Samples with high surface free energy are beneficial to the spreadability of the adhesive [24,25]. In this study, the contact angles of water (polar) and glycol (dispersive) were measured to evaluate the variation of the wettability of the counterparts, and Table 5 provides the surface tension components of the probe liquids (distilled water and glycol).

Table 5. Surface tension components of probe liquids (mJ/m^2) [24].

Wetting Liquids	γ_L	γ_L^d	γ_L^p
Distilled water	72.8	21.8	51.0
Glycol	48.3	29.3	19.0

The adhesion of liquid to the examined solid can be represented using the adhesion work W_a (Equation (1)), which represents the work required for the separation of the unit area of the interface between the tested liquid (L) and solid (S) [26,27].

$$W_a = \gamma_S + \gamma_L - \gamma_{SL} \quad (1)$$

where γ_S and γ_L represent the solid surface free energy and the liquid surface tension and γ_{SL} is the solid–liquid surface tension.

By combining with Young's equation represented by Equation (2), Equation (1) can be expressed as Equation (3) [26–28].

$$\gamma_S = \gamma_{SL} + \gamma_L \cos\theta \tag{2}$$

$$W_a = \gamma_L(1 + \cos\theta) \tag{3}$$

where θ represents the contact angle of the probe liquid.

W_a can also be represented as Equation (4). Consequently, surface free energy and its components can be worked out by Equations (5) and (6) [26,29,30].

$$W_a = 2\sqrt{\gamma_S^d \gamma_L^d} + 2\sqrt{\gamma_S^p \gamma_L^p} \tag{4}$$

$$\gamma_L(1 + \cos\theta) = 2\sqrt{\gamma_S^d \gamma_L^d} + 2\sqrt{\gamma_S^p \gamma_L^p} \tag{5}$$

$$\gamma_S = \gamma_S^p + \gamma_S^d \tag{6}$$

where γ_S^d and γ_S^p represent the dispersive and polar components of the examined solid, and γ_L^d and γ_L^p represent the dispersive and polar components of the tested liquid.

By solving Equations (5) and (6), the two components of surface free energy of the measured solid can be written separately as Equations (7) and (8).

$$\gamma_S^d = \left[\frac{\gamma_w\sqrt{\gamma_d^p}(1 + \cos\theta_w) - \gamma_d\sqrt{\gamma_w^d}(1 + \cos\theta_d)}{2\sqrt{\gamma_w^d\gamma_d^p} - 2\sqrt{\gamma_d^d\gamma_w^p}}\right]^2 \tag{7}$$

$$\gamma_S^p = \left[\frac{\gamma_w(1 + \cos\theta_w) - 2\sqrt{\gamma_S^d\gamma_w^d}}{2\sqrt{\gamma_w^p}}\right]^2 \tag{8}$$

The averaged contact angle values of distilled water and glycol are provided in Table 6 as well as the calculated results of surface free energy. It can be seen that the surface free energy of the Al alloy sample was greatly improved after laser treatment, in which the polar component was significantly increased, while the dispersion component was reduced. The difference in wettability of the Al–Li alloy surface was affected by the polar component and the dispersion component of the surface free energy. Specifically, at the laser scanning speeds of 25, 20, 15, 10, and 5 mm/s, the surface free energy of the samples increased by 133%, 170%, 192%, 169%, and 95%, respectively.

Table 6. Value of contact angles and surface free energy of the samples.

Samples	Contact Angle (°)		Polar Component (mJ/m^2)	Dispersive Component (mJ/m^2)	Surface Free Energy (mJ/m^2)
	Distilled Water	Glycol			
P-0	82.32	58.51	7.79	20.86	28.65
P-1	31.18	9.37	59.84	6.94	66.78
P-2	20.30	5. 66	73.44	4.00	77.44
P-3	12.07	4.04	80.74	2.81	83.55
P-4	20.92	6.94	72.99	4.04	77.03
P-5	41.79	11.12	43.37	12.60	55.97

The wettability of the solid surface was mainly determined by the microstructure and the chemical composition of the solid surface. The main reasons for the laser scanning of the Al alloy sample surface increasing the surface free energy are as follows: (1) During the laser processing, part of the energy diffused to the microtextured layer of the Al–Li alloy, which induced an increase in surface free energy, and then the R_a of the plate was

improved after laser pretreatment etching, which also induced an increase in surface free energy. According to the principle of similar compatibility [31], the microtextures with higher surface free energy are extremely compatible with water molecules that also have higher free energy, thus inducing the diffusion and spreading of water molecules; (2) As shown in Figure 6, after laser scanning, microstructures were formed in the dents with an uneven surface, which led to the increase in the capillary adsorption force [32]. The Van der Waals force between the microstructure and water molecules was enhanced [33], inducing the adsorption and spreading of the water molecule; (3) The laser excited the ionization of the Al alloy and the surrounding air, resulting in many functional groups of Al^{3+}, -OH with better hydrophilicity, and hence the surface free energy of the samples increased [14,34]. The measurement results of the sample surfaces' chemical composition (atomic ratio) is shown in Table 7.

Table 7. The measurement results of the sample surfaces' chemical composition.

Parameters	P-0	P-1	P-2	P-3	P-4	P-5
Al/at.%	93.45	86.03	86.07	85.92	85.71	84.82
O/at.%	5.42	12.07	12.64	12.75	13.40	13.77
Others/at.%	1.13	1.90	1.29	1.33	0.89	1.41

3.3. Adhesion Property

The values of adhesion strength are presented in Figure 7. As demonstrated in Figure 7, the strength of the bonded joints was largely influenced by laser surface pretreatment. The maximum shear strength of the joint was 27.64 MPa, appearing on the laser pretreatment sample with a scanning speed of 15 mm/s. The joint strength of the untreated sample was 13.37 MPa, at 25 mm/s. Under the scanning speeds of 20, 15, 10, and 5 mm/s, the bonding strength of the Al–Li alloy samples increased by 81%, 95%, 107%, 91%, and 78%, respectively. The fracture morphologies of joints pretreated by laser are shown in Figure 8 with the primitive joints as the contrast. As described in Figure 8, the failure mode of untreated Al–Li alloy adhesive joints was mainly apparent interfacial failure, and the PEEK adhesive layer was broken along the interface of the Al–Li alloy mainly, while the failure mode of the adhesive joints after laser scanning was mainly based on cohesive failure. Interfacial failure indicates that the surface adhesion of bonding joints is poor, while cohesive failure shows the surface adhesion of bonding joints is extraordinarily strong [28,35,36].

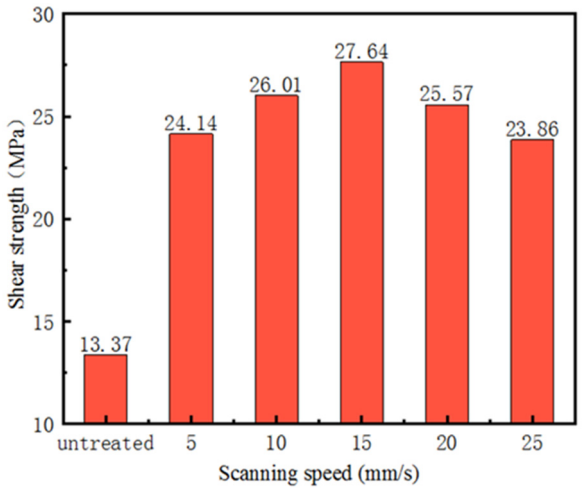

Figure 7. Shear strength values of the samples.

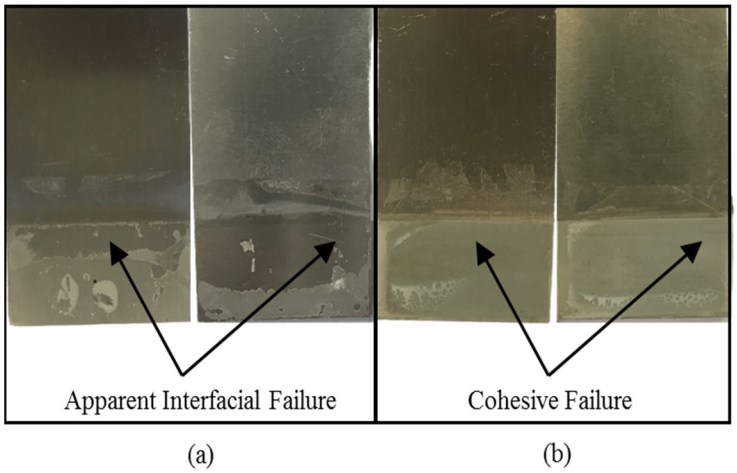

Figure 8. Fracture morphologies of the samples: (**a**) untreated, (**b**) laser scanning.

3.4. Relationships between Laser Scanning Speed, Surface Free Energy, and Shear Strength

In thermosetting composites, covalent chemical bonds are generally thought to take place and are considered the main adhesion mechanisms, whereas in thermoplastic composites mechanical interlocks are thought to be the dominating mechanisms [37]. The adhesive PEEK used in this research was a thermoplastic material, and the change of chemical composition on the surface of aluminum alloy by laser scanning was very small (as shown in Table 7), so we mainly explored the effect of surface treatment on the bonding performance from mechanical interlocks. The scanning speed of the femtosecond laser was adjusted to obtain different scanning energy on unit areas, thus adjusting the surface roughness and surface micromorphology of the Al–Li alloy. The microstructures were beneficial to the spreadability of the adhesive, improving the surface wettability, which was a nonnegligible factor that determined the bonding quality. However, the lower scanning speeds (higher scanning energy) did not equate to greater free energy of the sample surface and greater strength of the bonded joint. The lower the scanning speed, the greater the *Ra*. As the roughness increased, both the surface free energy and the shear strength increased rapidly at first and then decreased. The relationships between *Ra*, surface free energy, and shear strength are shown in Figure 9.

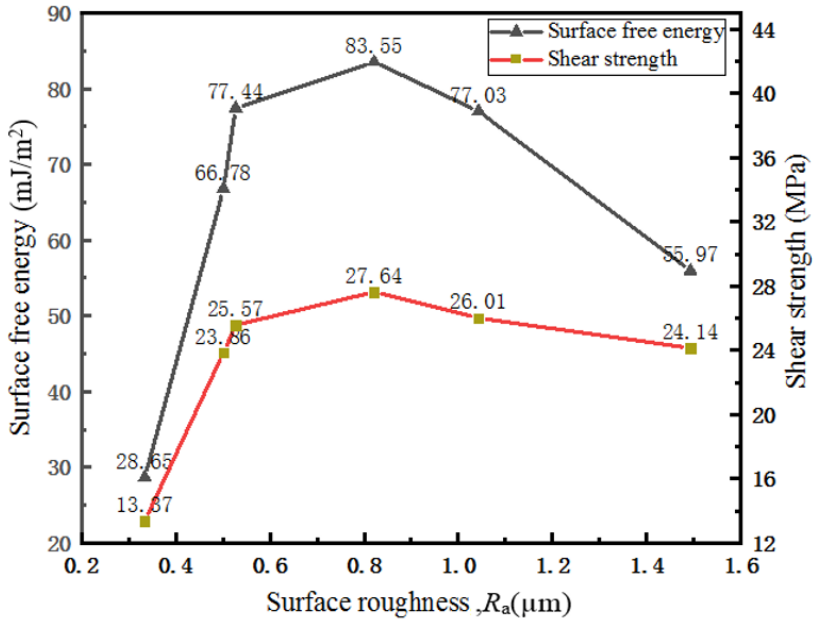

Figure 9. The relationships between *Ra*, surface free energy, and shear strength.

It is clear that the *Ra* value of 0.821 μm was an inflection point. Both surface free energy and shear strength increased with *Ra* before the *Ra* value of 0.821 μm, while they decreased with increasing roughness after 0.821 μm. Generally, the Pearson correlation coefficient is used to represent dependencies [38]. The correlation coefficient $\rho X, Y$, between two random variables X and Y with expected values μ_X and μ_Y and standard deviations σ_X and σ_Y can be described as:

$$\rho X, Y = \frac{E[(X - \mu_X)(Y - \mu_Y)]}{\sigma_X \sigma_Y} \quad (9)$$

where E is the expected value operator.

The closer the absolute value of $\rho X, Y$ is to 1, the stronger the relativity between the two random variables X and Y. Before the *Ra* value of 0.821 μm, the value $\rho X, Y$ of *Ra* and surface free energy was 0.835, and that of *Ra* and shear strength was 0.837, whereas the values are −0.995 and −0.988, respectively, after the *Ra* value of 0.821 μm. Obviously, the correlation between *Ra* and surface free energy and *Ra* and shear strength was stronger after 0.821 μm than before. This may indicate that the surface free energy and shear strength were influenced by both surface roughness and surface chemical composition at first, while surface roughness played a major role when the *Ra* was greater than 0.821 μm.

The increase in the groove depth increased the surface roughness, and the adhesive penetrated into the uniform groove, thereby increasing the actual contact area between the adhesive and the substrate. Due to the effect of the mechanical interlocks, the bonding performance can be improved [39]. However, excessive roughness or deep grooves may have a negative impact on the adhesion properties, especially if the grooves left by laser scanning are deep and narrow. Because these grooves may allow air to remain, making the adhesive unable to penetrate sufficiently into the grooves, the effect of mechanical interlocks between the agent and the substrate plate becomes weaker. Therefore the adhesive properties decrease [24]. Deep grooves are likely to form stress concentration inside the adhesive joint, which affects the quality of the bonding [15,40,41]. Therefore, when the scanning speed is over-low and the grooves left by laser scanning are over-deep, the surface free energy of the Al–Li alloy and the shear strength after bonding decrease instead. In addition, over-high scanning energy (scanning speed is over-low) will cause thermal damage to the surrounding tissues (as shown in Figure 6), which may negatively affect the material in depth, thereby affecting the free energy of the sample surface and the bonding strength. The relationships between the shear strength and surface free energy are shown in Figure 10, which shows that the value of shear strength increased as the surface free energy increased. These results suggest that samples with higher surface free energy may have higher shear strengths. Therefore, a surface with good wettability produced by pretreatment is crucial for obtaining high joint bonding strength.

In order to further explore the mechanism of the effect of femtosecond laser pretreatment on the bonding strength of Al–Li alloys, the scanning path of the laser was changed, and the previous perpendicular to stretch direction (Figure 1a) was changed to parallel to stretching direction (Figure 1b). Then, the subsequent bonding tensile experiment was conducted, and the results are shown in Figure 11. At the laser scanning speeds of 25, 20, 15, 10, and 5 mm/s, the strength of the Al alloy adhesive joint after pretreatment was 23.30, 25.13, 26.55, 24.51, and 22.92 MPa when scanning parallel to the tensile direction, reduced by 3.93%, 4.15%, 3.94%, 3.38%, and 3.48%, respectively, relative to scanning perpendicular to the tensile direction. It can be seen that the scanning path had a certain influence on the bonding strength of the Al–Li alloy, yet the effect was rather small. This indicates that the effect of femtosecond laser scanning of the Al–Li alloy surface on the bonding strength of the Al–Li alloy was mainly due to the laser pretreatment changing the wettability of the sample's surface, rather than from the mechanical interlock of macroscopic groove formed by the laser scanning on the bonding agent.

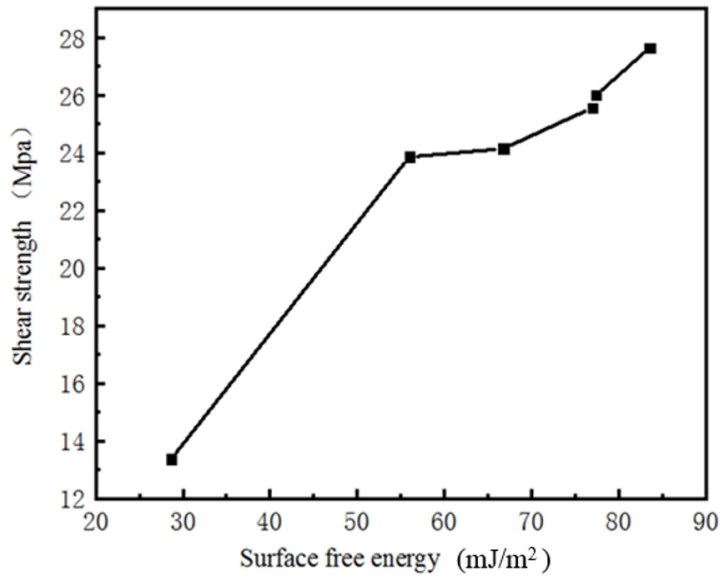

Figure 10. The shear strength of samples with different surface free energy.

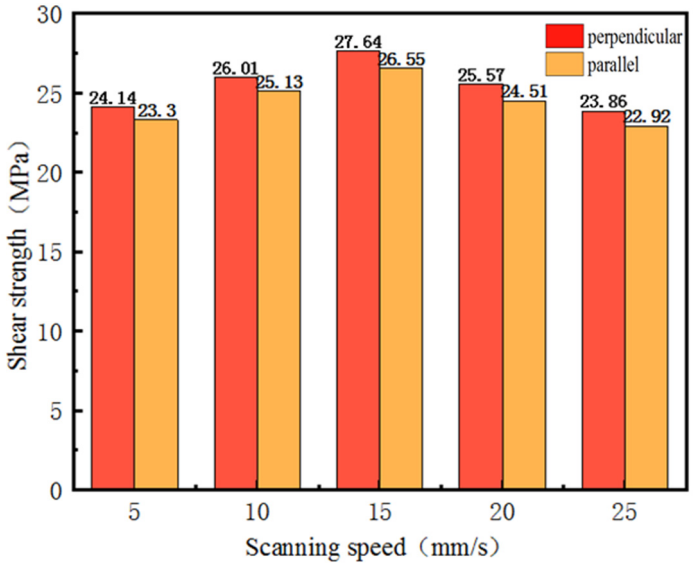

Figure 11. The shear strength of samples with different laser scanning paths.

4. Conclusions

In this work, an ultrafast femtosecond laser was introduced to increase surface wettability and strengthen the bonding joints; the conclusions are summarized as follows:

(1) Femtosecond laser etching of the Al–Li alloy surface had an important influence on its wettability. The surface wettability of samples could be changed by changing the laser scanning speed, and the surface free energy of the samples increased by 133%, 170%, 192%, 169%, and 95%, at the scanning speeds of 25, 20, 15, 10, and 5 mm/s, respectively.

(2) Femtosecond laser etching of the Al–Li alloy surface had an important influence on its bonding performance. The bonding strength of the Al–Li alloy samples increased by 81%, 95%, 107%, 91%, and 78%, at the scanning speeds of 25, 20, 15, 10, and 5 mm/s, respectively.

(3) Femtosecond laser etching of the Al–Li alloy surface mainly changed the surface roughness and surface micromorphology of the Al–Li alloy, thereby changing the surface free energy and bonding strength. Over-high (over-low scanning energy) and

over-low (over-high scanning energy) scanning speed reduced the surface free energy and bonding strength of the samples.

(4) Femtosecond laser etching improved the bonding performance of the Al–Li alloy mainly by improving the surface free energy of the samples, and its scanning path had a slight effect on the bonding strength (<5%).

Author Contributions: Conceptualization, Y.L.; methodology, J.C.; formal analysis, L.D.; investigation, J.C.; data curation, J.C.; writing—original draft preparation, J.C.; writing—review and editing, Y.L. and M.H.; project administration, Y.L. All authors have read and agreed to the published version of the manuscript.

Funding: This research was supported by the National Natural Science Foundation of China (Fundamental Research on One-step Hot Stamping Process of Large Al/PEEK/CFRP Hybrid Parts), the Guangxi Specially-invited Experts Foundation of Guangxi Zhuang Autonomous Region, China (GuiRenzi2019(13)), and the National Natural Science Foundation of China (51575535, 51662010).

Institutional Review Board Statement: Not applicable.

Informed Consent Statement: Not applicable.

Data Availability Statement: Not applicable.

Conflicts of Interest: The authors declare no conflict of interest.

References

1. Pramanik, A.; Basak, A.; Dong, Y.; Sarker, P.; Uddin, M.; Littlefair, G.; Dixit, A.R.; Chattopadhyaya, S. Joining of carbon fibre reinforced polymer (CFRP) composites and aluminium alloys—A review. *Compos. Part A Appl. Sci. Manuf.* **2017**, *101*, 1–29. [CrossRef]
2. Li, J.; Li, Y.; Huang, M.; Xiang, Y.; Liao, Y. Improvement of aluminum lithium alloy adhesion performance based on sandblasting techniques. *Int. J. Adhes. Adhes.* **2018**, *84*, 307–316. [CrossRef]
3. Zhang, C.; Chen, L.; Zhang, Y.; Wang, G.; Jin, J. Effect of laser processing microstructure on the bonding strength and failure mode of 7075-T6 aluminum alloy adhesive joints. *J. Manuf. Process.* **2021**, *66*, 302–312. [CrossRef]
4. Cui, J.; Wang, S.; Wang, S.; Chen, S.; Li, G. Strength and failure analysis of adhesive single-lap joints under shear loading: Effects of surface morphologies and overlap zone parameters. *J. Manuf. Process.* **2020**, *56*, 238–247. [CrossRef]
5. Sinmazçelik, T.; Avcu, E.; Bora, M.Ö.; Çoban, O. A review: Fibre metal laminates, background, bonding types and applied test methods. *Mater. Des.* **2011**, *32*, 3671–3685. [CrossRef]
6. Tiringer, U.; Kovač, J.; Milošev, I. Effects of mechanical and chemical pre-treatments on the morphology and composition of surfaces of aluminium alloys 7075-T6 and 2024-T3. *Corros. Sci.* **2017**, *119*, 46–59. [CrossRef]
7. Salstela, J.; Suvanto, M.; Pakkanen, T.T. Influence of hierarchical micro-micro patterning and chemical modifications on adhesion between aluminum and epoxy. *Int. J. Adhes. Adhes.* **2016**, *66*, 128–137. [CrossRef]
8. Lee, S.; Kim, D.; Kim, Y.; Jung, U.; Chung, W. Effect of aluminum anodizing in phosphoric acid electrolyte on adhesion strength and thermal performance. *Met. Mater. Int.* **2016**, *22*, 20–25. [CrossRef]
9. Won, S.J.; Kim, H.S. Effects of laser parameters on morphological change and surface properties of aluminum alloy in masked laser surface texturing. *J. Manuf. Process.* **2019**, *48*, 260–269. [CrossRef]
10. Feng, Z.; Zhao, H.; Tan, C.; Zhu, B.; Xia, F.; Wang, Q.; Chen, B.; Song, X. Effect of laser texturing on the surface characteristics and bonding property of 30CrMnSiA steel adhesive joints. *J. Manuf. Process.* **2019**, *47*, 219–228. [CrossRef]
11. Wan, H.; min, J.; Lin, J.; Carlson, B.E.; Maddela, S.; Sun, C. Effect of laser spot overlap ratio on surface characteristics and adhesive bonding strength of an Al alloy processed by nanosecond pulsed laser. *J. Manuf. Process.* **2021**, *62*, 555–565. [CrossRef]
12. Li, Y.; Meng, S.; Gong, Q.; Huang, Y.; Gan, J.; Zhao, M.; Liu, B.; Liu, L.; Zou, G.; Zhuang, D. Experimental and theoretical investigation of laser pretreatment on strengthening the heterojunction between carbon fiber-reinforced plastic and aluminum alloy. *ACS Appl. Mater. Interfaces* **2019**, *11*, 22005–22014. [CrossRef]
13. Spadaro, C.; Sunseri, C.; Dispenza, C. Laser surface treatments for adhesion improvement of aluminium alloys structural joints. *Radiat. Phys. Chem.* **2007**, *76*, 1441–1446. [CrossRef]
14. Wu, Y.; Lin, J.; Carlson, B.E.; Lu, P.; Balogh, M.P.; Irish, N.P.; Mei, Y. Effect of laser ablation surface treatment on performance of adhesive-bonded aluminum alloys. *Surf. Coat. Technol.* **2016**, *304*, 340–347. [CrossRef]
15. Romoli, L.; Moroni, F.; Khan, M. A study on the influence of surface laser texturing on the adhesive strength of bonded joints in aluminium alloys. *CIRP Ann.* **2017**, *66*, 237–240. [CrossRef]
16. Phillips, K.C.; Gandhi, H.H.; Mazur, E.; Sundaram, S.K. Ultrafast laser processing of materials: A review. *Adv. Opt. Photon.* **2015**, *7*, 684–712. [CrossRef]
17. Chichkov, B.N.; Momma, C.; Nolte, S.; Von Alvensleben, F.; Tünnermann, A. Femtosecond, picosecond and nanosecond laser ablation of solids. *Appl. Phys. A Mater. Sci. Process.* **1996**, *63*, 109–115. [CrossRef]

18. Pan, L.; Pang, X.; Wang, F.; Huang, H.; Shi, Y.; Tao, J. Effect of surface micro-pits on mode-II fracture toughness of Ti-6Al-4V/PEEK interface. *Compos. Struct.* **2019**, *229*, 111333. [CrossRef]
19. Sun, Z.; Huang, M. Fatigue crack propagation of new aluminum lithium alloy bonded with titanium alloy strap. *Chin. J. Aeronaut.* **2013**, *26*, 601–605. [CrossRef]
20. Li, J.; Li, Y.; Xiang, Y.; Chen, J. Effect of low-velocity impact on the strength and durability of bonded joint in hygrothermal environment. *J. Adhes.* **2020**, 1–16. [CrossRef]
21. Hertveldt, I.; Cooman, B.C.D.; Meseure, K.; Xhoffer, C. ASTM D1002-72 Standard test method for strength properties of adhesive in shear by tension loading (metal-to-metal), 1983. *ISIJ Int.* **1999**, *39*, 1280–1288. [CrossRef]
22. Amoruso, S.; Ausanio, G.; Barone, A.C.; Bruzzese, R.; Gragnaniello, L.; Vitiello, M.; Wang, X. Ultrashort laser ablation of solid matter in vacuum: A comparison between the picosecond and femtosecond regimes. *J. Phys. B At. Mol. Opt. Phys.* **2005**, *38*, L329–L338. [CrossRef]
23. Fan, P.; Bai, B.; Zhong, M.; Zhang, H.; Long, J.; Han, J.; Wang, W.; Jin, G. General strategy toward dual-scale-controlled metallic micro–nano hybrid structures with ultralow reflectance. *ACS Nano* **2017**, *11*, 7401–7408. [CrossRef] [PubMed]
24. Xu, Y.; Li, H.; Shen, Y.; Liu, S.; Wang, W.; Tao, J. Improvement of adhesion performance between aluminum alloy sheet and epoxy based on anodizing technique. *Int. J. Adhes. Adhes.* **2016**, *70*, 74–80. [CrossRef]
25. Zhang, X.; Zhang, Y.; Ma, Q.; Dai, Y.; Hu, F.; Wei, G.; Xu, T.; Zeng, Q.; Wang, S.; Xie, W. Effect of surface treatment on the corrosion properties of magnesium-based fibre metal laminate. *Appl. Surf. Sci.* **2017**, *396*, 1264–1272. [CrossRef]
26. Baldan, A. Adhesion phenomena in bonded joints. *Int. J. Adhes. Adhes.* **2012**, *38*, 95–116. [CrossRef]
27. Park, S.-J.; Cho, M.-S.; Lee, J.-R. Studies on the surface free energy of carbon–carbon composites: Effect of filler addition on the ilss of composites. *J. Colloid Interface Sci.* **2000**, *226*, 60–64. [CrossRef]
28. Zheng, R.; Lin, J.; Wang, P.-C.; Zhu, C.; Wu, Y. Effect of adhesive characteristics on static strength of adhesive-bonded aluminum alloys. *Int. J. Adhes. Adhes.* **2015**, *57*, 85–94. [CrossRef]
29. Dalet, P.; Papon, E.; Villenave, J.-J. Surface free energy of polymeric materials: Relevancy of conventional contact angle data analyses. *J. Adhes. Sci. Technol.* **1999**, *13*, 857–870. [CrossRef]
30. Shang, J.; Flury, M.; Harsh, J.B.; Zollars, R.L. Comparison of different methods to measure contact angles of soil colloids. *J. Colloid Interface Sci.* **2008**, *328*, 299–307. [CrossRef]
31. Tian, F.; Li, B.; Ji, B.; Yang, J.; Zhang, G.; Chen, Y.; Luo, Y. Antioxidant and antimicrobial activities of consecutive extracts from Galla chinensis: The polarity affects the bioactivities. *Food Chem.* **2009**, *113*, 173–179. [CrossRef]
32. Van Honschoten, J.W.; Brunets, N.; Tas, N.R. Capillarity at the nanoscale. *Chem. Soc. Rev.* **2010**, *39*, 1096–1114. [CrossRef]
33. Bico, J.; Tordeux, C.; Quere, D. Rough wetting. *Europhys. Lett.* **2001**, *55*, 214–220. [CrossRef]
34. Kim, J.G.; Choi, I.; Gil Lee, D. Contact angle and wettability of hybrid surface-treated metal adherends. *J. Adhes. Sci. Technol.* **2013**, *27*, 794–810. [CrossRef]
35. Flanagan, J.; Schütze, P.; Dunne, C.; Twomey, B.; Stanton, K.T. Use of a blast coating process to promote adhesion between aluminium surfaces for the automotive industry. *J. Adhes.* **2018**, *96*, 580–601. [CrossRef]
36. Zheng, R.; Lin, J.; Wang, P.-C.; Wu, Q.; Wu, Y. Effects of a sheet metal stamping lubricant on static strength of adhesive-bonded aluminum alloys. *J. Adhes. Sci. Technol.* **2015**, *29*, 1382–1402. [CrossRef]
37. Mathijsen, D. The black magic of carbon fiber reinforced thermoplastics. *Reinf. Plast.* **2015**, *59*, 185–189. [CrossRef]
38. Rudawska, A.; Danczak, I.; Müller, M.; Valasek, P. The effect of sandblasting on surface properties for adhesion. *Int. J. Adhes. Adhes.* **2016**, *70*, 176–190. [CrossRef]
39. Bresson, G.; Jumel, J.; Shanahan, M.E.; Serin, P. Strength of adhesively bonded joints under mixed axial and shear loading. *Int. J. Adhes. Adhes.* **2012**, *35*, 27–35. [CrossRef]
40. Prolongo, S.G.; Rosario, G.; Ureña, A. Study of the effect of substrate roughness on adhesive joints by SEM image analysis. *J. Adhes. Sci. Technol.* **2006**, *20*, 457–470. [CrossRef]
41. Prolongo, S.G.; del Rosario, G.; Ureña, A. Comparative study on the adhesive properties of different epoxy resins. *Int. J. Adhes. Adhes.* **2006**, *26*, 125–132. [CrossRef]